Supplementary Information (SI) for Journal of Materials Chemistry A.

Supporting Information

Constructing Multiple Microstructure in Sb_2Te_3-based Thermoelectrics Enables High-performance Segmented Power Generator

Min Wang [a,b],† Qiang Zhang [b,e],†* Yue Wu [c],† Ruyuan Li [a,b], Qiaoyan Pan [b,e], Jingtao Xu [d], Dongxiang Lv [c], Xiaojian Tan [b,e],* Guo-Qiang Liu [b,e], Jun Jiang [b,e],*

[a] School of Material Science and Chemical Engineering, Ningbo University; Ningbo 315211, China.

[b] Ningbo Institute of Materials Technology and Engineering, Chinese Academy of Sciences; Ningbo, 315201, China.

[c] No. 18th Research Institute, China Electronics Technology Group Corporation; Tianjin, 300392, China.

[d] School of Materials and Chemical Engineering, Ningbo University of Technology; Ningbo 315211, China.

[e] University of Chinese Academy of Sciences; Beijing, 100049, China.

† These authors contribute equally.

* Corresponding authors.

E-mail addresses: qiangzhang@nimte.ac.cn (Q. Zhang), tanxiaojian@nimte.ac.cn (X. Tan), jjun@nimte.ac.cn (J. Jiang).

1. The calculation of κ_{ph} and κ_{bip}

In the low-temperature region (~200 K), the contribution of the bipolar diffusion effect to the phonon scattering is very small. Therefore, in the low temperature region (~200 K) above Debye temperature (θ_{D} = 94 K)[1], the lattice thermal conductance κph of the material is calculated by using Wiedemann-Franz law ($\kappa_{\mathrm{ph}} = \kappa_{\mathrm{tot}} - L\sigma T$), ignoring the effect of intrinsic excitation. Subsequently, κ_{ph} is extrapolated to the temperature region above 250 K according to the relationship between κ_{ph} and $1/T$. The κ_{ph} and κ_{bip} calculated by this method are in good agreement with the experimental data, which shows that the hypothesis and extrapolation of the appeal are reasonable[2].

2. Debye-Callaway model

The lattice thermal conductivity of materials is limited by many factors, and the relationship between these factors can be explained through the Debye-Callaway model[3]:

According to the model, the lattice thermal conductivity κ_{ph} is defined as[4]:

$$\kappa_{ph} = \frac{k_B}{2\pi^2 v}\left(\frac{k_B T}{\hbar}\right)^3 \int_0^{\Theta_D/T} \tau_{\mathrm{tot}}(x)\frac{x^4 e^x}{\left(e^x - 1\right)^2}dx$$

where the integrand term represents the spectral lattice thermal conductivity κ_{s}:

$$\kappa_{\mathrm{s}} = \frac{k_{\mathrm{B}}}{2\pi^2 v}\left(\frac{k_{\mathrm{B}}T}{\hbar}\right)^3 \frac{x^4 e^x}{\tau_{tot}^{-1}(x)\left(e^x - 1\right)^2}$$

where x, k_{B}, $\hbar$ v θ_{D} τ_{tot} are the reduced phonon frequency (x= $\mu_{\omega}/k_{\mathrm{B}}T$), k_{B} is the Boltzmann constant, the reduced Plank constant, the average speed of acoustic phonon, the Debye temperature, and the total phonon scattering relaxation time, τ_{tot} can be derived in accordance with Matthiessen's rule[5]:

$$\tau_{\mathrm{tot}}^{-1} = \tau_{\mathrm{U}}^{-1} + \tau_{\mathrm{PD}}^{-1} + \tau_{\mathrm{GB}}^{-1} + \tau_{\mathrm{D}}^{-1} + \tau_{\mathrm{SP}}^{-1}$$

The main phonon scattering mechanisms in the sample include Umklapp phonon-phonon scattering (U), point-defect scattering (PD), grain boundary scattering (GB), dislocation scattering (DS), and nanoprecipitate scattering (NP).

The relaxation time associated with Umklapp phonon-phonon scattering (τ_U) is given by:

$$\tau_U^{-1} = A_N \frac{2}{\left(6\pi^2\right)^{1/3}} \frac{k_B V^{1/3} \gamma^2 \omega^2 T}{M v^3}$$

where V is the atomic volume, γ is the Grüneisen parameter, and M is the atomic mass.

The relaxation time related to point defect scattering (τ_{PD}) is computed from:

$$\tau_{PD}^{-1} = \frac{V\omega^4}{4\pi v^3}\Gamma$$

where Γ is point defect scattering parameter and can be expressed as:

$$\Gamma = x(1-x)\left[\left(\frac{\Delta M}{M}\right)^2 + \frac{2}{9}\left\{(G + 6.4\gamma)\frac{1+r}{1-r}\right\}^2\left(\frac{\Delta a}{a}\right)^2\right]$$

where x is the fractional concentration of either of constituents, ΔM is the difference in mass, G is the parameter representing a ratio of fractional change of bulk modulus to that of local bond length, r is Poisson's ratio, and Δa is the difference in lattice constant, respectively.

The relaxation time related to grain boundary scattering (τ_{GB}) is computed from:

$$\tau_{GB}^{-1} = \frac{v}{d}$$

The relaxation time related to dislocation scattering (τ_{DS}) is computed from:

$$\tau_{DS}^{-1} = 0.6 B_D^2 N_D (\gamma + \Delta\gamma)^2 \omega \left\{\frac{1}{2} + \frac{1}{24}\left(\frac{1-2r}{1-r}\right)^2\left[1 + \sqrt{2}\left(\frac{\upsilon_L}{\upsilon_T}\right)\right]^2\right\} + N_D \frac{V^{4/3}}{v^2}\omega^3$$

where, N_D is dislocation density, B_D is effective Burger's vector, $\Delta\gamma$ is change in

Grüneisen parameter, v_L is vertical acoustic phonon speed, v_T is transverse acoustic phonon speed.

The modified scattering due to dislocation strain can be calculated by changing the initial γ by adding a change in the Grüneisen parameter ($\Delta\gamma$) due to the impurity atmosphere:

$$\Delta\gamma = \frac{V_{ST}C_0K}{k_BT_a}(\gamma\alpha^2 - \alpha\beta)$$

$$\alpha = \frac{V_{BT} - V_{ST}}{V_{ST}}$$

$$\beta = \frac{M_{ST} - M_{BT}}{2M_{ST}}$$

where C_0, K, T_a are concentration of In_2Te_3 in Sb_2Te_3, bulk modulus, sample sintering temperature, respectively.

The relaxation time related to nanoprecipitate scattering (τ_{SP}) is computed from:

$$\tau_{SP}^{-1} = v\left[\left(2\pi R^2\right)^{-1} + \left(\frac{4}{9}\pi R^2(\Delta D/D)^2(\omega R/v)^4\right)^{-1}\right]^{-1}N_P$$

where, D is the mass density of the host, ΔD is the density difference between the host and nanoscale second phase precipitations, R is the average radius of the second phase, and Np is the number density of the second phase.

The relevant parameters are summarized in **Table S2**.

3. Single Parabolic Band model

Assuming that the phonon scattering mechanism is dominant, based on a single parabolic band model[6], the Seebeck coefficient S only depends on the reduced Fermi level η:

$$S = \pm\frac{k_B}{e}\left(\frac{F_1^2}{F_0^2} - \eta\right)$$

The carrier concentration n_H and carrier mobility μ_H can be calculated according to the following equation:

$$n_H = \frac{16\pi\left(2m_d^* k_B T\right)^{1.5}}{3h^3}\frac{F_0^2}{F_{-0.5}}$$

$$\mu_H = \mu_0\frac{F_{-0.5}(\eta)}{2F_0(\eta)}$$

The electrical conductivity can be expressed as:

$$\sigma = \frac{8\pi e\left(2k_B T m_d^*\right)^{1.5}\mu_0}{3h^3}F_0 = \frac{8\pi e\left(2k_B T m_0\right)^{1.5}\mu_W}{3h^3}F_0$$

In the above equations, F_j is the Fermi integral:

$$F_j = \int_0^\infty \frac{x^j dx}{1 + e^{(x-\eta)}}$$

4. Multi-physics field simulations

Based on the TE effect module of COMSOL software, the conversion efficiency of TE modules in thermal balance is calculated by establishing a steady-state model. Based on the *p*-type Sb_2Te_3, *p*-type $(Bi,Sb)_2Te_3$ and *n*-type $Bi_2Te_{2.7}Se_{0.3}$ materials prepared by zone melting in this experiment, the model of a TE module including insulating ceramic substrate, copper electrode, TE leg and load is established. The theoretical conversion efficiency and output power at 350 K temperature difference are simulated by adjusting the section ratio of *p*- and *n*-legs, the surface length ratio of leg length and total cross section area. The relevant parameters of the model are shown in **Table S3**.

5. Error analysis of thermoelectric module output performance measurements

The measurement error associated with conversion efficiency using the home-built instrument can be analyzed through standard error analysis and propagation methods. Specifically, the uncertainty in thermal conductivity measurements for copper is 5%, while the uncertainties for A_{Cu}, l_{Cu}, I, U and T are 0.5%, 1.5%, 0.5%, 0.5%, and ±0.1%, respectively. The uncertainty is calculated using the following equations:

$$\delta(\Delta T_{Cu}) = \sqrt{\left[T_{Cu1} \times \delta(T_{Cu1})\right]^2 + \left[T_{Cu2} \times \delta(T_{Cu2})\right]^2}/(T_{Cu1} - T_{Cu2})$$

$$\delta(Q) = \sqrt{\delta(\Delta T_{Cu})^2 + \delta(\kappa_{Cu})^2 + \delta(A_{Cu})^2 + \delta(l_{Cu})^2}$$

$$\delta(P) = \sqrt{\delta(I)^2 + \delta(U)^2}$$

$$\delta(P + Q) = \sqrt{[P \times \delta(P)]^2 + [Q \times \delta(Q)]^2}/(P + Q)$$

$$\delta(\eta) = \sqrt{\delta(P)^2 + \delta(P + Q)^2}$$

Consequently, the uncertainty in conversion efficiency is approximately 6%, which is consistent with findings reported in the literature (*Nat. Commun.* **2024**, 15, 1468).

6. The electronic quality factor (B_{E})

The electronic quality factor (B_{E}) serves as a pivotal metric to evaluate the interplay between the Seebeck coefficient (S) and electrical conductivity (σ) in thermoelectric materials, while uncovering the underlying mechanisms governing electrical performance optimization, such as band structure engineering, carrier scattering dynamics, and bipolar effects. It is mathematically defined as:

$$B_E = S^2\sigma/\left[\frac{S_r^2 exp(2 - S_r)}{1 + exp[-5(S_r - 1)]} + \frac{S_r\pi^2/3}{1 + exp[5(S_r - 1)]}\right]$$

where $S_r = \frac{|S|}{k_B/e}$, with k_B denoting the Boltzmann constant and e the elementary charge.

For ideal thermoelectric materials, B_{E} exhibits weak temperature dependence. Consequently, deviations in B_{E} as a function of temperature provide critical insights into intrinsic material behaviors, including: Valence Band Convergence, Carrier Scattering Mechanisms, Bipolar Effects.

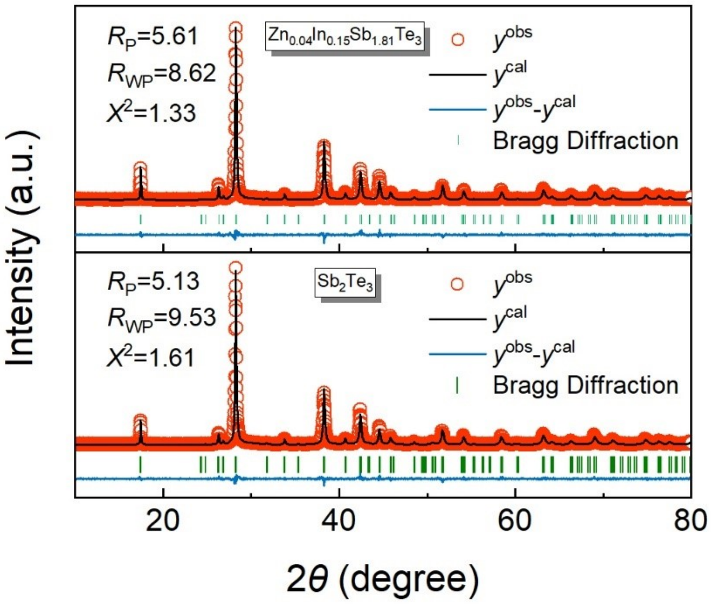

Figure S1. Rietveld refinement XRD pattern of pristine Sb_2Te_3 and $Zn_{0.04}In_{0.15}Sb_{1.81}Te_3$ materials.

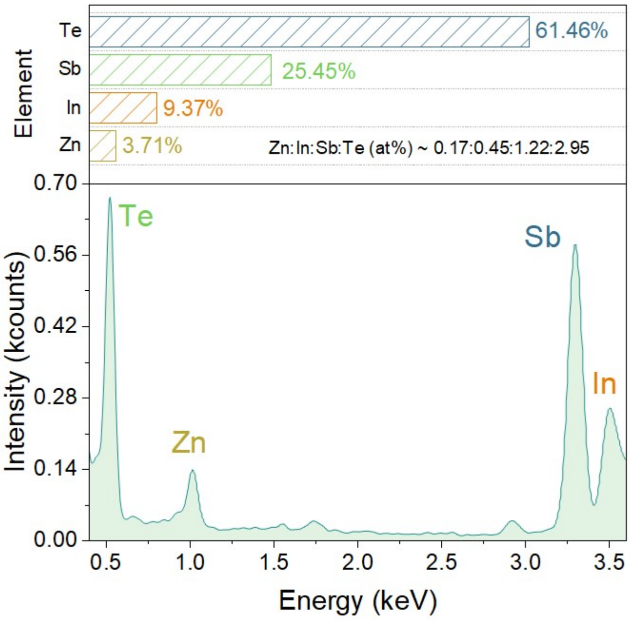

Figure S2. Element scan results for Figure 2F region.

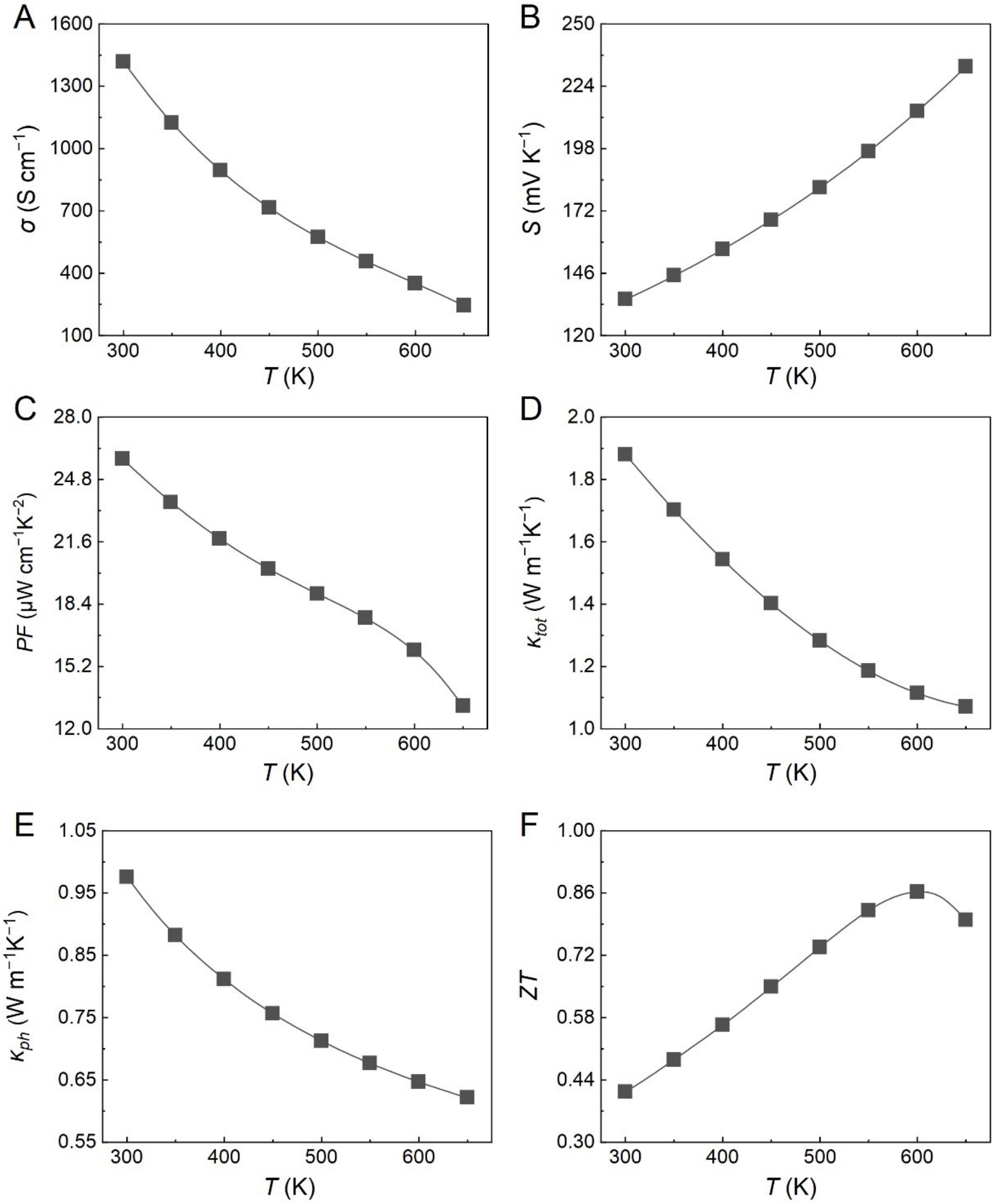

Figure S3. Temperature dependence of (**A**) electrical conductivity, (**B**) Seebeck coefficient, (**C**) power factor, (**D**) total thermal conductivity, (**E**) lattice thermal conductivity, and (**F**) *ZT* of the pristine Sb_2Te_3 sample.

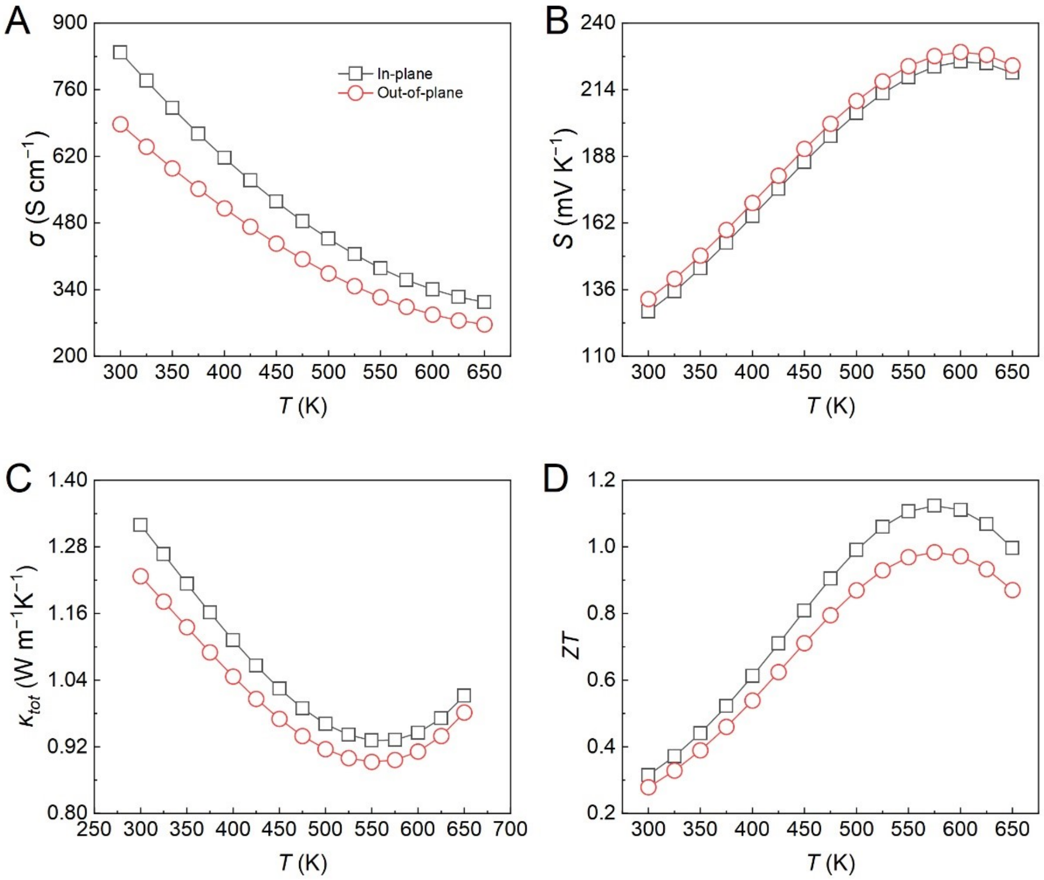

Figure S4. Comparison of electronic and thermal transport properties of sample $Zn_{0.04}In_{0.15}Sb_{1.81}Te_3$ along the out-of-plane and in-plane directions for (**A**) electrical conductivity, (**B**) Seebeck coefficient, (**C**) total thermal conductivity and (**D**) *ZT* value.

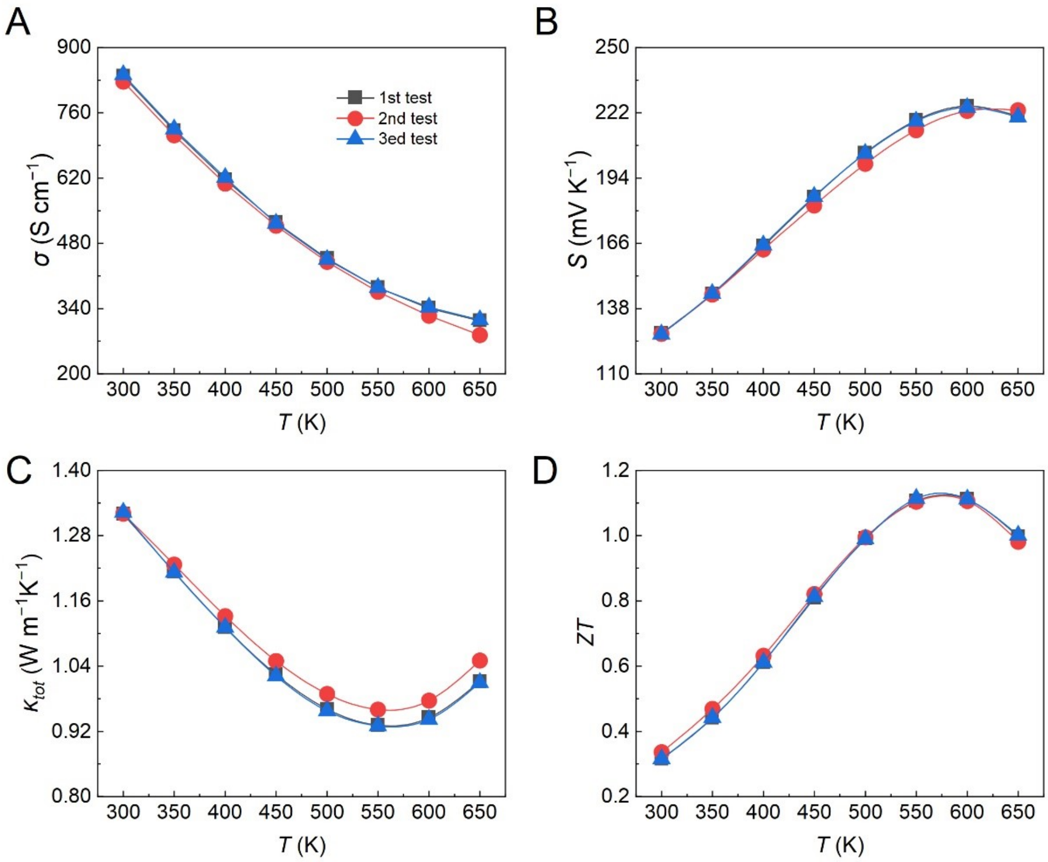

Figure S5. The temperature dependence of (**A**) electrical conductivity, (**B**) Seebeck coefficient, (**C**) total thermal conductivity, and (**D**) *ZT* values for the $Zn_{0.04}In_{0.15}Sb_{1.81}Te_3$ sample is investigated for three times, revealing consistently excellent results.

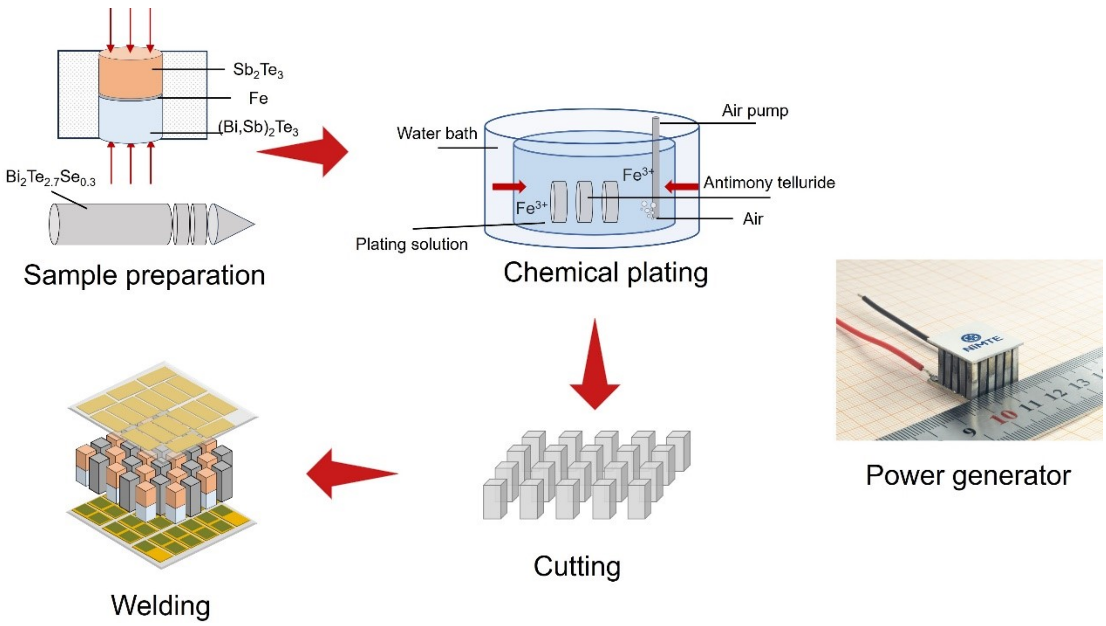

Figure S6. Schematic diagram of key manufacturing processes for TE generator production. It should be noted that the barrier layer here is not applied through conventional electroplating but rather through an optimized chemical plating process, ensuring excellent bonding strength.

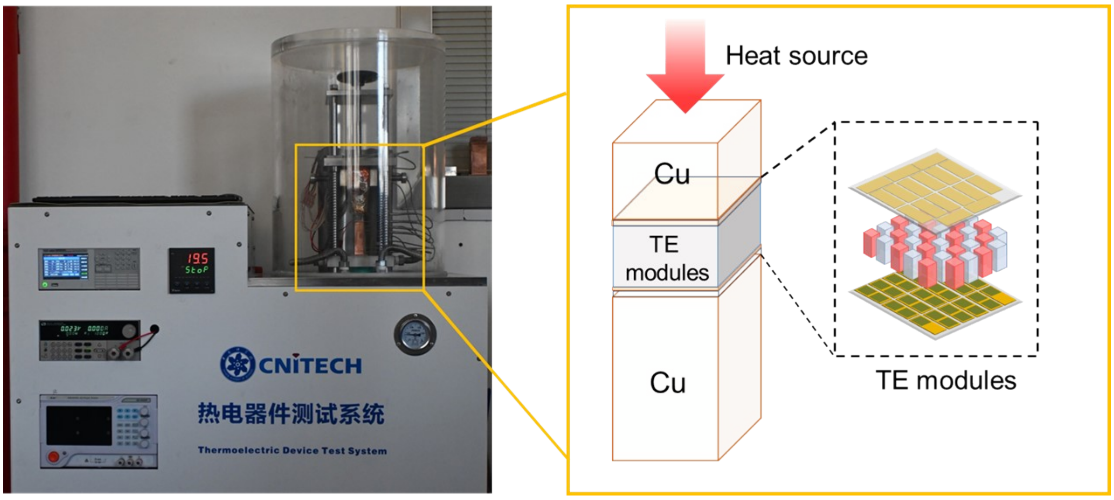

Figure S7. A home-made system for testing the heat-to-electric output characteristics of TE modules.

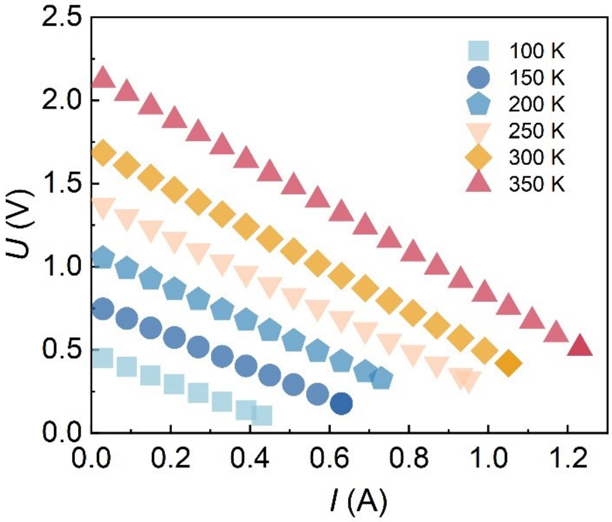

Figure S8. The relationship between the output voltage and current obtained by the test.

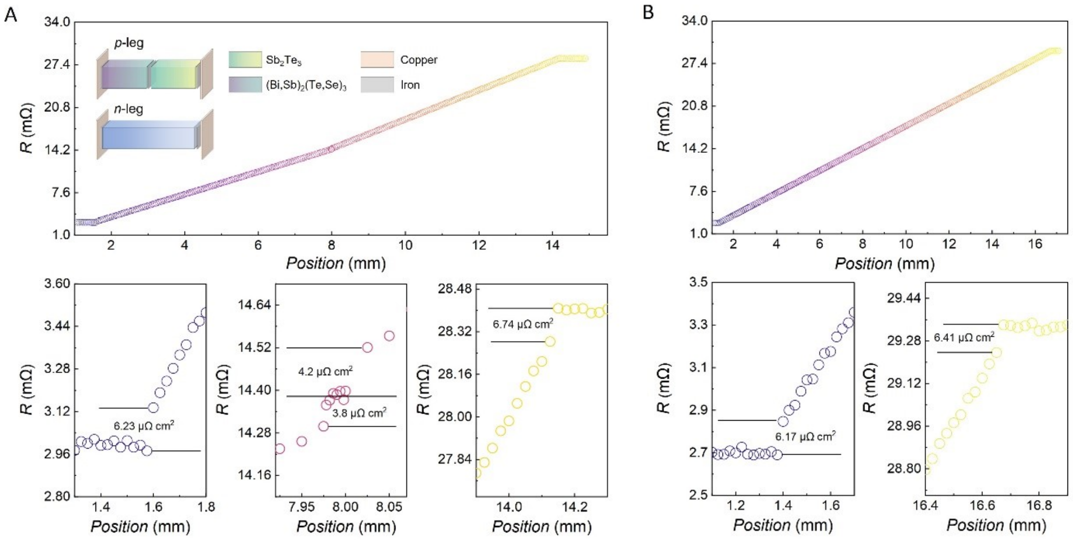

Figure S9. Evaluation of contact resistances at different interfaces of (**A**) segmented *p*-legs and (**B**) single *n*-legs.

Table S1. Lattice parameters of the $Zb_xIn_ySb_{2-x-y}Te_3$ samples obtained from XRD refinement results.

Samples		Lattice parameters (Å)		
x	y	a	b	c
0	0	4.97022	4.97022	30.75591
0.02		4.9688	4.9688	30.75587
0.04		4.96432	4.96432	30.68631
0.06		4.96432	4.96432	30.65334
0.04	0.003	4.96208	4.96208	30.65165
	0.006	4.96208	4.96208	30.63436
	0.009	4.95984	4.95984	30.61708

Table S2. Parameters for calculating κ_{ph} of the $Zn_{0.04}In_{0.15}Sb_{1.81}Te_3$ sample in the Debye-Callaway model.

Parameters	Description	Values	Ref.
θ_D	Debye temperature	94 K	4
B_D	Effective Burger's vector	1.12×10^{-8} m	fitted
v_L	Longitudinal phonon velocity	2844 m s^{-1}	3
v_T	Transverse phonon velocity	1780 m s^{-1}	5
v	In-plane average velocity of phonon	2333 m s^{-1}	5
γ	Grüneisen parameter	2.3	5
r	Poisson's ratio	0.24	7
V	Average atomic volume of Sb_2Te_3	30.77 $Å^3$	7
V_{BT}	Atomic volume of In_2Te_3	3.03×10^{-29} m^3	
V_{ST}	Atomic volume of Sb_2Te_3	3.13×10^{-29} m^3	
M_{BT}	Atomic mass of In_2Te_3	2.01×10^{-25} kg	
M_{ST}	Atomic mass of Sb_2Te_3	2.07×10^{-25} kg	
C_0	Concentration of In_2Te_3 in Sb_2Te_3	0.15	
K	Bulk modulus	53.2 GPa	4
T_a	Sample Sintering temperature	723 K	Exp.
d	Grain size	1.5×10^{-6} m	Exp.
N_d	Dislocation density	5.84×10^{14} cm^{-2}	Exp.
R	Average radius of second phase	10 nm	Exp.
N_P	Number density of Second phase	8×10^{12} m^3	Exp.
D	Density of matrix	6.3 g/cm^3	Exp.

Table S3. Parameters used to calculate theoretical conversion efficiency and output power.

Parameters	Value
Cold side temperature	300 K
Hot side temperature	650 K
Contact resistivity	6 μΩ cm^2
Thickness of copper electrode	0.3 mm
Thickness of ceramic plate	0.9 mm

Table S4. Temperature dependence of electrical conductivity, Seebeck coefficient, total thermal conductivity for *p*-type SPS-sintered $(Bi,Sb)_2Te_3$ and *n*-type zone-melted $Bi_2Te_{2.7}Se_{0.3}$ from our previous report[8].

Material	T (K)	σ *(S cm^{-1})*	S (μV K^{-1})	κ_{tot} (W m^{-1}K^{-1})
p-type SPS-sintered $(Bi,Sb)_2Te_3$	300	1095.89096	198.63019	0.93089
	350	830.00286	213.05973	0.87411
	400	649.02046	218.0382	0.88686
	450	538.3455	210.8277	0.97287
	500	483.37971	188.69032	1.13589
n-type zone-melted $Bi_2Te_{2.7}Se_{0.3}$	300	1354.69173	-208.37738	1.48882
	350	1123.02437	-217.5744	1.44864
	400	962.35283	-216.33003	1.59664
	450	862.95509	-205.93836	1.88641
	500	815.10913	-187.69348	2.27153
	550	809.09292	-162.88947	2.70557
	600	835.18443	-132.82043	3.14211
	650	-98.78044	883.66164	3.53473

Reference:

1 V. D. Blank, S. G. Buga, V. A. Kulbachinskii, V. G. Kytin, V. V. Medvedev, M. Yu. Popov, P. B. Stepanov and V. F. Skok, *Phys. Rev. B*, 2012, **86**, 075426.

2 F. Hao, P. Qiu, Y. Tang, S. Bai, T. Xing, H.-S. Chu, Q. Zhang, P. Lu, T. Zhang, D. Ren, J. Chen, X. Shi and L. Chen, *Energy Environ. Sci.*, 2016, **9**, 3120–3127.

3 F. Yang, T. Ikeda, G. J. Snyder and C. Dames, *J. Appl. Phys.*, 2010, **108**, 034310.

4 D. Bessas, I. Sergueev, H.-C. Wille, J. Perßon, D. Ebling and R. P. Hermann, *Phys. Rev. B*, 2012, **86**, 224301.

5 X. Chen, H. D. Zhou, A. Kiswandhi, I. Miotkowski, Y. P. Chen, P. A. Sharma, A. L. Lima Sharma, M. A. Hekmaty, D. Smirnov and Z. Jiang, *Appl. Phys. Lett.*, 2011, **99**, 261912.

6 D. M. Rowe, Ed., *CRC handbook of thermoelectrics*, CRC Press, Boca Raton, FL, 1995.

7 E. S. Toberer, A. Zevalkink and G. J. Snyder, *J. Mater. Chem.*, 2011, **21**, 15843.

8 W. Huang, X. Tan, J. Cai, S. Zhuang, C. Zhou, J. Wu, G. Liu, B. Liang and J. Jiang, *Mater. Today Phys.*, 2023, **32**, 101022.